The Astrophysical Journal, 700:L145–L148, 2009 August 1 doi:10.1088/0004-637X/700/2/L145

IMAGING SPECTROPOLARIMETRY WITH IBIS: EVOLUTION OF BRIGHT POINTS IN THE QUIET SUN

B. Viticchié[1], D. Del Moro[1], F. Berrilli[1], L. Bellot Rubio[2], and A. Tritschler[3]
[1] Dipartimento di Fisica, Università degli Studi di Roma "Tor Vergata," Via della Ricerca Scientifica 1, I-00133 Rome, Italy; bartolomeo.viticchie@roma2.infn.it
[2] Instituto de Astrofísica de Andalucía (CSIC), Apdo. de Correos 3004, 18080 Granada, Spain
[3] National Solar Observatory/Sacramento Peak, P.O. Box 62, Sunspot, NM 88349, USA
Received 2009 April 17; accepted 2009 June 22; published 2009 July 15

ABSTRACT

We present the results from first spectropolarimetric observations of the solar photosphere acquired at the Dunn Solar Telescope with the Interferometric Bidimensional Spectrometer. Full Stokes profiles were measured in the Fe I 630.15 nm and Fe I 630.25 nm lines with high spatial and spectral resolutions for 53 minutes, with a Stokes V noise of 3×10^{-3} the continuum intensity level. The data set allows us to study the evolution of several magnetic features associated with G-band bright points (BPs) in the quiet Sun. Here we focus on the analysis of three distinct processes, namely the coalescence, fragmentation, and cancellation of G-band BPs. Our analysis is based on an SIR inversion of the Stokes I and V profiles of both Fe I lines. The high spatial resolution of the G-band images combined with the inversion results helps to interpret the undergoing physical processes. The appearance (dissolution) of high-contrast G-band BPs is found to be related to the local increase (decrease) of the magnetic filling factor, without appreciable changes in the field strength. The cancellation of opposite-polarity BPs can be the signature of either magnetic reconnection or the emergence/submergence of magnetic loops.

Key words: Sun: magnetic fields – Sun: photosphere – techniques: polarimetric

1. INTRODUCTION

The improvements in accuracy and spatial resolution of modern spectropolarimeters have led to a new concept of quiet-Sun magnetism. It has been shown, for example, that quiet-Sun magnetic fields have strengths from 0 to 2 kG and that their evolution is closely related to the granular plasma motions (e.g., Lin & Rimmele 1999; Domínguez Cerdeña et al. 2003).

However, the formation and disappearance of magnetic concentrations in the quiet Sun are not yet well understood, mainly because of the difficulty of obtaining time sequences of polarization measurements over large fields of view (FOVs). The recent upgrade of the Interferometric Bidimensional Spectrometer (IBIS; Cavallini 2006) to a vector polarimeter makes it ideally suited to study these processes with high spatial, spectral, and temporal resolution.

Here we analyze IBIS polarimetric measurements showing the temporal evolution of kG fields associated with G-band bright points (BPs) as these interact with the photospheric plasma. Our aim is to improve the current knowledge about BP evolution in relation to magnetic fields (Berger et al. 1995; Berger & Title 2001; Nisenson et al. 2003; Sánchez Almeida et al. 2004). We focus on poorly known processes like the coalescence, fragmentation, and cancellation of G-band BPs. This study exploits the physical parameters derived from both the observed profiles and the inversion results.

2. OBSERVATIONS

The observations were taken with IBIS at the NSO/Dunn Solar Telescope on 2006 November 21 from 16:24 UT to 17:17 UT. The data set consists of 36 scans of the Fe I 630.15 nm and Fe I 630.25 nm lines with 89 s cadence, obtained at disk center. The two spectral lines are sampled with a total of 45 wavelengths (FWHM = 2 pm) on an equidistant grid of 2.3 pm skipping the telluric line in between the two Fe I lines, but sampling the O_2 630.28 nm which allows to set the absolute wavelength scale.

In spectropolarimetric mode, the incoming light to IBIS is modulated by a pair of nematic liquid crystal variable retarders placed in a collimated beam in front of the field stop of the instrument. The light is analyzed by a beam splitter in front of the detector, imaging two orthogonal states onto the same chip thus allowing for dual-beam spectropolarimetry. The modulation is in such a way that at each wavelength position six modulation states $I+S$ (and its orthogonal states $I-S$) are detected with the following temporal scheme: $S = [+V, -V, +Q, -Q, +U, -U]$.

The pixel scale of the spectropolarimetric images is 0.″18, while the integration time per modulation state and wavelength was 80 ms. For each narrowband filtergram, a simultaneous broadband (633.32 ± 5 nm) counterpart was acquired, imaging the same FOV with the same exposure time. Furthermore, G-band filtergrams (430.5 ± 0.5 nm) with approximately the same FOV, but smaller pixel scale (0.″037) were taken with an exposure time of 15 ms. The seeing during the acquisition run was excellent and stable, allowing the adaptive optics system (Rimmele 2004) to achieve near-diffraction-limited performance.

The broadband and G-band images have been restored via Multi-Frame Blind Deconvolution (MFBD; Löfdahl 2002) to further reduce the seeing degradation and obtain a homogeneous resolution in the whole $50'' \times 50''$ FOV.

The global and local shifts necessary to align and destretch the broadband images with respect to the MFBD restored broadband images have been computed and applied onto the spectropolarimetric images. This process reduces the seeing-induced crosstalk and makes the spatial resolution of the whole spectropolarimetric scan comparable with that of the individual narrowband filtergrams.

The data set was then corrected for the systematic wavelength shift across the FOV (Reardon & Cavallini 2008) caused by the collimated mounting of the Fabry–Perots and for instrumental polarization introduced by the telescope and the polarimeter itself. The average noise level for Stokes V has been measured to be $\sigma_V = 3 \times 10^{-3}$ in units of the continuum intensity.

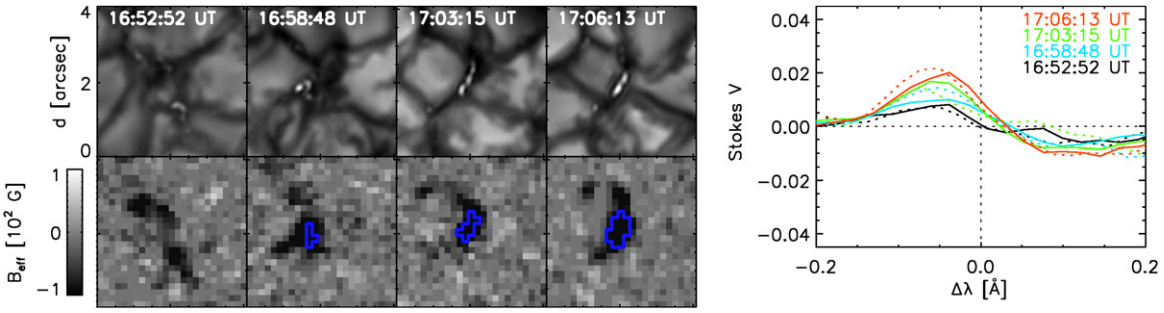

Figure 1. Selection of four instants from the BP coalescence process. First row: *G*-band filtergram. Second row: COG magnetic flux density (images are saturated at 100 G). Contour plot: kG fields regions as obtained from the inversion analysis of Stokes *V* profiles above 4 × σ_V. Right plot: Fe I 630.15 nm (dotted line) and Fe I 630.25 nm (solid line) Stokes *V* profiles calculated as an average over a 0.″5 × 0.″5 box around the position of the strongest magnetic flux densities for each instant. Stokes *V* profiles are normalized to the continuum intensity.

The *G*-band observations are aligned with the broadband images by using grid line targets. We then registered the different scans via a correlation procedure to eliminate residual global shifts due to tracking inaccuracies.

3. DATA ANALYSIS

We estimate the longitudinal magnetic flux density applying the center-of-gravity method (COG; Rees & Semel 1979) to the observed Stokes *V* profiles of the Fe I 630.15 nm line. Unlike the classical magnetograph formula, the COG technique does not suffer from saturation effects in the kG regime.

To determine the intrinsic field strengths and magnetic filling factors associated with the *G*-band BPs, we perform an inversion of the Stokes *I* and *V* profiles of the two lines with the SIR code (Ruiz Cobo & del Toro Iniesta 1992). We defer the interpretation of the linear polarization to future work with a more specific analysis as recommended by Lites et al. (2008).

The inversion is based on two atmospheric components, one magnetized and the other field free. The fractional area of the pixel occupied by the former (the magnetic filling factor *f*) is a free parameter of the inversion. The temperature stratification of each component is modified with two nodes, using the stratification of the Harvard-Smithsonian Reference Atmosphere (Gingerich et al. 1971) as initial guess. The line-of-sight (LOS) velocities in the two components as well as the field strength in the magnetized component are assumed to be constant with height. The stray-light contamination is modeled by averaging the Stokes *I* spectra in a region of 1″ around the inverted profile. This average profile is added to the observed spectra weighted by a factor α; the stray-light factor distribution is in good agreement with Orozco Suárez et al. (2007) with typical value of $\alpha = 80\%$. The macroturbulence and microturbulence velocities are set to zero. In the inversion process, the finite spectral resolution of the instrument is taken into account using the spectral point-spread function of IBIS (Reardon & Cavallini 2008).

Since our goal is to study the evolution of strong kG flux concentrations associated with *G*-band BPs, we invert only those profiles whose Stokes *V* signals are above 4 × σ_V in both Fe I lines; such regions always enclose *G*-band BPs. A total of 53, 000 profiles meet this condition, corresponding to approximately 3% of the whole FOV at any step of the time sequence.

4. EVOLUTION OF MAGNETIC FEATURES

This sequence of high spectral and spatial resolution observations allows us to study the coalescence, fragmentation, and cancellation of small-scale magnetic structure. Examples of these processes are identified by inspecting the MFBD-restored *G*-band time series taken as context data in addition to the spectropolarimetric observations.

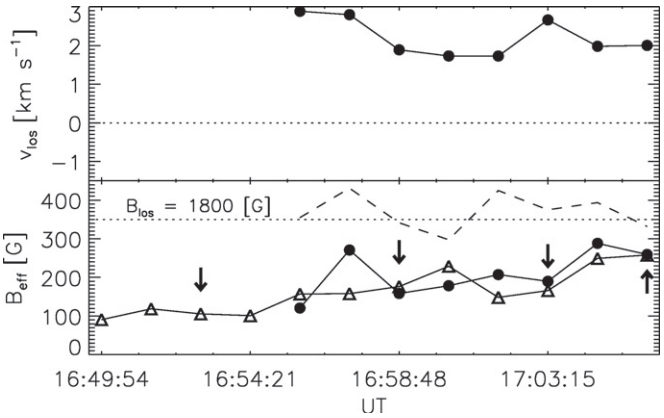

Figure 2. Evolution of relevant quantities for the BP coalescence process with full temporal resolution. Upper panel: velocity along the LOS obtained from the inversion; positive (negative) values mean photospheric downflows (upflows). Lower panel: magnetic flux density calculated via COG method (triangles) and from the inversion (dots); we also plot the magnetic field strength obtained from the inversion, appropriately rescaled (dashed line); the horizontal dotted line is a reference level for the field strength. The black arrows mark the instants shown in Figure 1.

Figures 1, 3, and 5 exemplify each individual process with a selection of four *G*-band subfields (4″ × 4″) (first row), simultaneous, and co-spatial maps of COG magnetic flux density (second row) and Stokes *V* profiles (right plot) averaged over a 0.″5 × 0.″5 box centered on the strongest COG signal. The contour lines overlaid on the magnetic flux density delimit kG field regions as indicated by the inversion of both Fe I lines.

Figures 2 and 4 display plots of several quantities relevant to the processes shown in Figures 1 and 3 with full temporal resolution. We report the evolution of the LOS velocity for the magnetized component ($v_{\rm los}$), the magnetic flux density ($B_{\rm eff}$) and LOS field strength ($B_{\rm los}$). $v_{\rm los}$ and $B_{\rm los}$ are outputs of the inversion analysis, while $B_{\rm eff}$ has been computed from both the inversion as $f \times B_{\rm los}$ (dots) and from the COG magnetic flux density (triangles). The plotted quantities are averaged in the same 0.″5 × 0.″5 box defined above.

4.1. Coalescence

In Figure 1 a BP coalescence process is shown. In the first frame a diffuse magnetic signal can be recognized in the

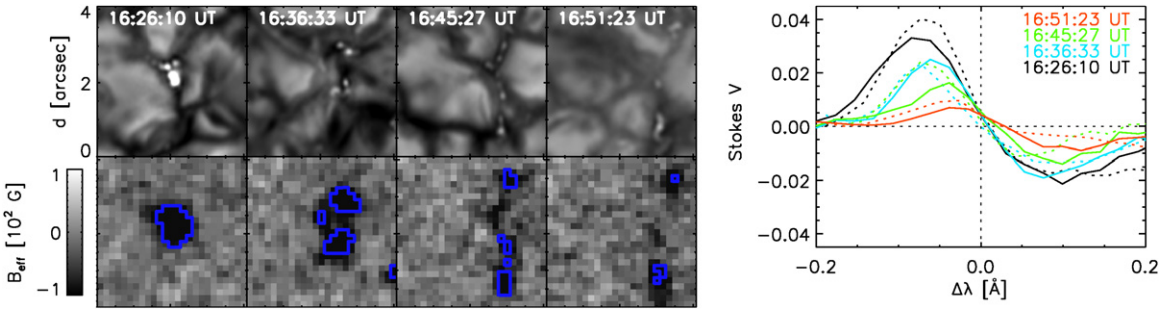

Figure 3. Selection of four instants from the BP fragmentation process. Same as Figure 1.

magnetic flux density images. In the *G*-band filtergram, scattered, low-contrast bright features associated with the diffuse magnetic signals are recognizable. The photospheric advection field gathers the initially diffuse magnetic features in a small region of about 0.″5; simultaneously, in the same region, a BP emerges in the intergranular lane and kG fields are revealed by the inversion procedure (Stokes *V* profiles emerge above $4 \times \sigma_V$).

In a time interval of about 10 minutes, the magnetic flux density more than doubles (Figure 2). Simultaneously, the BP extends over 0.″5 in the intergranular lane. The LOS velocity is between 2 and 3 km s^{-1}. The magnetic field strength remains nearly constant at about 1.8 kG, while the magnetic flux density increases in good agreement with the same quantity calculated via COG method (Figure 2). These results indicate that the increase in Stokes *V* amplitude is due to the increase in the magnetic filling factor and not due to an increase in the field strength; the inversion analysis retrieves an increase in *f* from about 5% to about 14%. A confirmation of this result comes from Stokes *V* amplitudes in Figure 1: since the beginning of the sequence, the Stokes *V* profiles of the two Fe I lines have comparable amplitudes, so the field is always in the kG regime.

4.2. Fragmentation

Figure 3 shows the fragmentation of a BP. In a time interval of about 25 minutes, a high-contrast BP is fragmented in many small-scale bright features that move all over an intergranular lane with a length of about 4″. The Stokes *V* signals are reduced in this process, but the comparable Stokes *V* amplitudes of the two Fe I lines indicate again a kG regime.

Figure 4 shows that the magnetic field strength remains constant at about 1.6 kG, while the smearing of the "progenitor" BP causes a decrease in the magnetic flux density from about 400 G to about 80 G. These results suggest that the magnetic filling factor is reduced by the action of the photospheric advection field; in fact the inversion analysis retrieves a decrease in *f* from about 13% to about 4%. The LOS velocity exhibits smaller values than in the BP coalescence case; more specifically, it varies around 1 km s^{-1}.

4.3. Cancellation

The process we present in Figure 5 shows the cancellation of opposite-polarity BPs converging over the same photospheric region.

The photospheric advection field gathers together opposite polarity flux concentrations. The result is a rapid disappearance of the *G*-band BPs and the complete cancellation of the magnetic signals. The whole process lasts about 25 minutes. In the plot of Figure 5, we report Fe I 630.25 nm Stokes *V* profiles associated

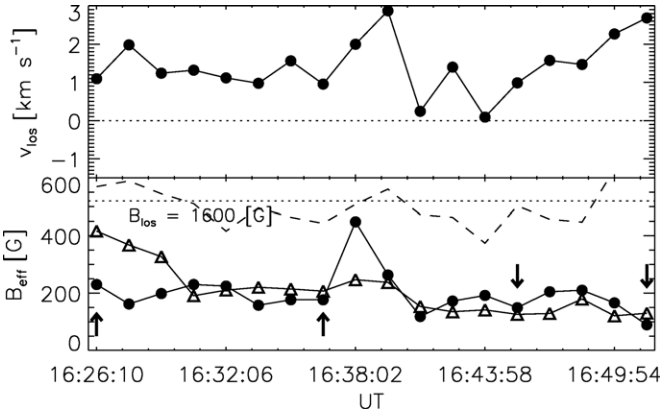

Figure 4. Evolution of relevant quantities for the BP fragmentation process with full temporal resolution. Same as Figure 2.

with both polarity BPs. From the gradual reduction of the profile amplitudes we conclude that a continuous process is causing the disappearance of the circular polarization signals.

5. DISCUSSION AND CONCLUSIONS

Recently, Nagata et al. (2008) and Bello González et al. (2009) presented analyses of events in which the amplification of Stokes *V* signal was found to be simultaneous to the appearance of bright features in continuum and broadband images, respectively. Nagata et al. (2008) performed an inversion of both Fe I 630 nm lines and measured an increase in the magnetic field strength associated with very strong redshifts (up to 6 km s^{-1}). The authors showed how Stokes *V* profiles evolved during the amplification process, changing from a sub-kG regime (Fe I 630.15 nm Stokes *V* amplitude lower than the Fe I 630.25 nm one) to a kG regime (the Stokes *V* profiles of the two lines have comparable amplitudes). All these aspects are compatible with a convective collapse process. Bello González et al. (2009) also observed an increase in the Stokes *V* signal in the Fe I 617.3 nm line and tentatively suggested the occurrence of a convective collapse.

The approach adopted in the present work shows that the inversion of the observed profiles can help to interpret the physical process behind such observations. In particular, the increase of the filling factor reported in Section 4.1 is induced by the action of the photospheric advection field. By the same token, the fragmentation event described in Section 4.2 and associated with a decrease of the kG field filling factor, is produced by an opposite driving action of the advection field. Furthermore, the more stable velocity in Figure 2 suggests that the gathering of bright features in the coalescence process takes place in a steady downflow, while the variability of the velocity in

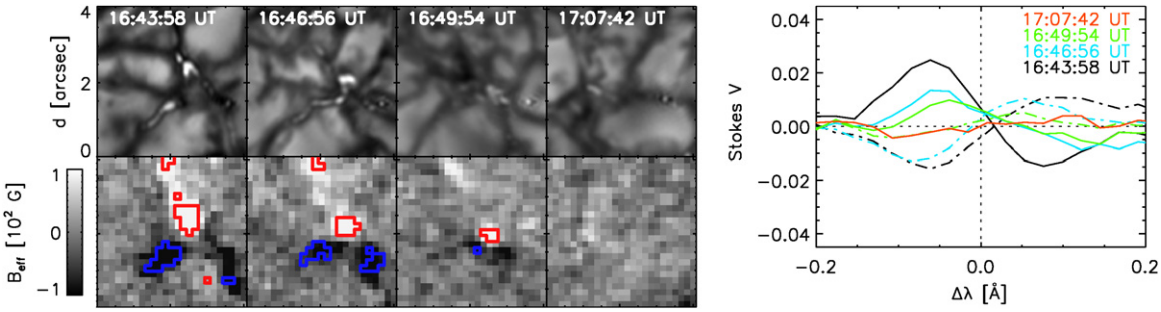

Figure 5. Selection of four instants from the BP cancellation process. First row: *G*-band filtergram. Second row: COG magnetic flux density (images are saturated at 100 G). Contour plot: kG fields regions as obtained from the inversion analysis of Stokes *V* profiles; positive (red contours) and negative (blue contours) polarity regions are represented. Right plot: Fe I 630.25 nm Stokes *V* profiles calculated as average over a 0.″5 × 0.″5 box around the position of the minimum (solid line) and maximum (dot-dashed line) magnetic flux densities for each time instant. Stokes *V* profiles are normalized to the continuum intensities. For 17:07:42 UT a single 0.″5 × 0.″5 box fixed at the interaction point is used to calculate the average profiles.

Figure 4 suggests that such a stability is lost during the fragmentation process. In both cases, the contrast of *G*-band BPs is strictly correlated to the fraction of atmosphere filled by kG fields, and therefore controlled by the advection field.

Different scenarios can explain the cancellation process. The first is the interaction, via successive magnetic reconnections, between opposite-polarity field lines belonging to different magnetic bundles. A second possible scenario is the emergence of a U-shaped magnetic loop or the submergence of a Ω-shaped loop whose footpoints are observed as BPs. In both scenarios, a certain amount of linear polarization is expected to be found between the circularly polarized regions, during the cancellation phase. Contrary to this expectation, IBIS was not able to detect any trace of linear polarization. Higher polarimetric accuracy seems to be required to investigate this issue.

We have presented results obtained from first observations with IBIS in spectropolarimetric mode. They provide new information on three distinct and poorly known processes, namely the coalescence, fragmentation, and cancellation of flux concentrations in the photosphere of the quiet Sun. Our analysis highlights the importance of interpreting Stokes profiles via inversion techniques to identify the physical mechanisms behind the processes under examination. In this way, we have been able to associate the appearance (dissolution) of high-contrast *G*-band BPs with a local increase (decrease) in the filling factor of photospheric kG fields induced by the photospheric advection field. Apparently, the field strength does not undergo significant variations in those processes (Figures 2 and 4). Also, we have analyzed the cancellation of opposite-polarity *G*-band BPs. Our results add further data to the recent observation of interactions between granular flows and magnetic elements acquired with *HINODE* (e.g., Zhang et al. 2009).

We are very grateful to the anonymous referee for the constructive comments and remarks on the manuscript. This work was partially supported by the MAE Spettro-Polarimetria Solare Bidimensionale research project, by the Agenzia Spaziale Italiana through grant ASI-ESS, by the Istituto Nazionale di Astrofisica through grant PRIN-INAF 2007, by the Spanish MICINN through project ESP2006-13030-C06-02 and by Junta de Andalucía through project P07-TEP-2687. The authors are grateful to the DST observers D. Gilliam, M. Bradford, and J. Elrod. IBIS was built by INAF-Osservatorio Astrofisico di Arcetri with contributions from the Università di Firenze and the Università di Roma "Tor Vergata." The authors acknowledge F. Cavallini, K. Reardon, and the IBIS team for their invaluable and unselfish support. NSO is operated by the Association of Universities for Research in Astronomy, Inc. (AURA), under cooperative agreement with the National Science Foundation.

REFERENCES

Bello González, N., Yelles Chaouche, L., Okunev, O., & Kneer, F. 2009, A&A, 494, 1091
Berger, T. E., & Title, A. M. 2001, ApJ, 553, 449
Berger, T. E., et al. 1995, ApJ, 454, 531
Cavallini, F. 2006, Sol. Phys., 236, 415
Domínguez Cerdeña, I., Sánchez Almeida, J., & Kneer, F. 2003, A&A, 407, 741
Gingerich, O., Noyes, R. W., Kalkofen, W., & Cuny, Y. 1971, Sol. Phys., 18, 347
Lin, H., & Rimmele, T. 1999, ApJ, 514, 448
Lites, B. W., et al. 2008, ApJ, 672, 1237
Löfdahl, M. G. 2002, arXiv:astro-ph/0209004
Nagata, S., et al. 2008, ApJ, 677, L145
Nisenson, P., van Ballegooijen, A. A., de Wijn, A. G., & Sütterlin, P. 2003, ApJ, 587, 458
Orozco Suárez, D., et al. 2007, ApJ, 670, L61
Reardon, K. P., & Cavallini, F. 2008, A&A, 481, 897
Rees, D. E., & Semel, M. D. 1979, A&A, 74, 1
Rimmele, T. R. 2004, in Proc. SPIE 5490, 34
Ruiz Cobo, B., & del Toro Iniesta, J. C. 1992, ApJ, 398, 375
Sánchez Almeida, J., et al. 2004, ApJ, 609, L91
Zhang, J., Yang, S., & Jin, C. 2009, arXiv:0905.1553